CIRP Annals - Manufacturing Technology 72 (2023) 501–504

Contents lists available at ScienceDirect

CIRP Annals - Manufacturing Technology

journal homepage: https://www.editorialmanager.com/CIRP/default.aspx

Surface integrity and superelastic response of additively manufactured Nitinol after heat treatment and finish machining

R. Bertolini[a], S. Bruschi (1)[a,*], A. Ghiotti (1)[a], E. Savio (1)[a], L. Ceseracciu[b], I.S. Jawahir (1)[c]

[a] Department of Industrial Engineering (DII), University of Padova, Via Venezia 1, 35131 Padova, Italy
[b] Materials Characterization Facility, Istituto Italiano di Tecnologia (IIT), Via Morego, 30, Genova 16163, Italy
[c] Institute for Sustainable Manufacturing (ISM), University of Kentucky, Lexington, KY 40506, USA

ARTICLE INFO

Article history:
Available online 12 April 2023

Keywords:
Additive manufacturing
Cryogenic machining
Nitinol

ABSTRACT

This paper explores the feasibility of adopting additive manufacturing followed by heat treatment and finish machining to fabricate Nitinol components with enhanced surface integrity and more favourable superelastic characteristics. The most suitable manufacturing approach is demonstrated to achieve these characteristics by establishing appropriate bulk and surface conditioning. New insights are presented on the correlation of process chain parameters and Nitinol superelastic response focusing on the role of the microstructural constituents and surface integrity generated from finish machining with different cooling conditions. The wear behaviour of Nitinol components fabricated by the proposed manufacturing approach is also evaluated to demonstrate bearing applications.

1. Introduction

Nickel-titanium alloys, Nitinol in particular, are exploited in numerous biomedical, actuation and sensing applications due to their unique characteristics such as shape memory effect (SME), superelasticity (SE), biocompatibility, low stiffness, high fatigue and wear resistance [1]. Manufacturing of Nitinol parts must be capable to guarantee such characteristics during the part service life. However, the SME and SE properties, which strongly depend on the alloy transformation temperatures, can be significantly influenced by the manufacturing chain, thus making the part suitable for specific applications. Therefore, it is important to study and establish the Nitinol capabilities in terms of both the process chain steps and the operating parameters.

In recent years, additive manufacturing (AM) techniques have been designed and optimized to fabricate parts made of Nitinol, showing great application potential in terms of complexity-for-free [2], and making the concept of 4D printing exploitable. In the latter, the fourth D stands for time, namely the 3D printed part made of a shape memory alloy, such as Nitinol, can have a controlled change in geometry in response to an externally applied stress stimulus [3]. The Nitinol SME and SE have often been addressed by investigating how the AM parameters may affect them, especially in terms of transformation temperatures [4]. However, most of the published literature presents findings of Nitinol just with a single processing step, as is AM, neglecting the cumulative interactions and influences that different subsequent steps may have on its resulting characteristics. In particular, the combined thermal effects of the different processing steps and their significant influence on the Nitinol transformation temperatures, which, in turn, can affect its SME and SE properties, is a case point.

Amongst post-AM operations, finish machining steps are often mandatory to assure the part's final geometry and properties. However, most of the published papers dealing with Nitinol machining and investigating the influence of the cutting parameters on its characteristics just refer to the alloy in the wrought state [5]. In [6] a Ni-rich wrought Nitinol was machined under orthogonal cutting conditions showing an alteration of both the microstructure and transformation behaviour up to a depth of 400–500 μm below the machined surface, and stating that machining must be taken into account since it affects the overall material behaviour. The same wrought Nitinol was studied in [7] showing a strong relationship between the cutting speed and phase transformation response during machining.

In this context, the aim of the paper is to evaluate the surface integrity and superelastic response of a Ni-rich Nitinol during a process chain including: (i) AM to fabricate the near-net-shape part, (ii) heat treating to modify the microstructure, and (iii) final finish machining to condition the surface. For the first time, a whole process chain is contemplated, proving a correlation between the process chain parameters and the Nitinol superelastic response, with a focus on the role of the microstructural constituents and surface integrity. The Nitinol wear behaviour is also assessed to evaluate how it can be influenced by the material characteristics induced by the investigated process chain.

2. Experimental work

The process chain implemented in this study to evaluate the characteristics of a Ni-rich Nitinol (hereafter named NiTi) is shown in Fig. 1 and it includes: (i) AM through the laser powder bed fusion (LPBF) technique to fabricate the near-net-shape part, (ii) heat

* Corresponding author at: University of Padova Department Industrial Engineering, Department of Industrial Engineering, Via Venezia 1, 35131 Padova, Italy.
E-mail address: stefania.bruschi@unipd.it (S. Bruschi (1)).

https://doi.org/10.1016/j.cirp.2023.04.025

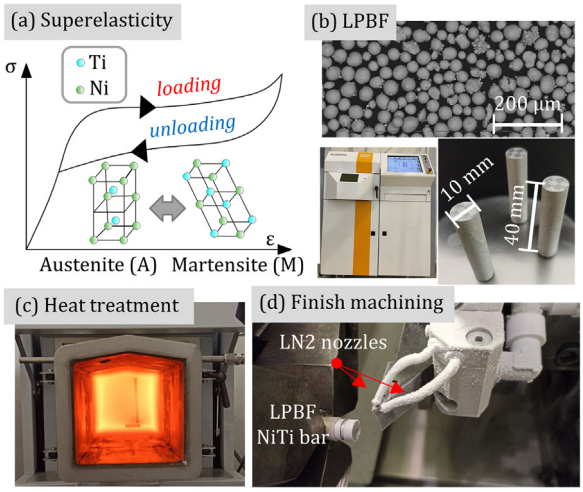

Fig. 1. NiTi SE (a); LPBF (b); heat treatment (c); finish machining (d).

treating to enhance the material SE, and (iii) finish machining to obtain the net-shape part and condition its surface. The same figure shows also the stress-strain path illustrating the mechanically-induced superelasticity (also known as pseudo-elasticity), intended as the material capability to undergo large deformations (more than 3%) that are fully recoverable when applying mechanical loading between austenite finish A_f temperature and M_d, which is the temperature at which martensite can no longer be stress-induced.

$Ni_{50.8}Ti_{49.2}$ (at%) powders with a size of 15–45 µm from ECKART TLS™, produced by gas atomization from cast ingots, were used for LPBF on a Sisma MYSINT™ 100 machine. The adopted LPBF parameters (Table 1) were optimized in a previous study [8] to assure the highest density and austenitic microstructure at room temperature, being austenite the phase assuring SE to NiTi.

Table 1
LPBF parameters optimized for Ni-rich NiTi.

Power	Scanning speed	Hatch distance	Layer thickness	Input energy density
P (W)	V (mm/s)	d_h (mm)	t (mm)	E (J/mm^3)
70	1100	0.06	0.025	42.42

Cylinders of 10 mm diameter and 40 mm height were printed vertically, namely with the axis parallel to the building direction (BD), using the island scanning strategy, and then mechanically removed from the base plate. Then, some cylinders were heat treated to emphasize the SE behaviour by inducing the precipitation of Ni-rich precipitates. To this aim, the samples were first subjected to a solution treatment at 1060 °C for 60 min and rapidly cooled in water. Then, a batch of samples was subjected to ageing treatment at T = 300 °C (T3), while another one at T = 600 °C (T6). In both cases, the ageing treatment lasted 180 min and was followed by air cooling.

Finally, as-built (AB), T3 and T6 samples were longitudinally turned on a Mori Seiki™ CNC lathe using VCEX 110301L-F 1125 inserts. The finishing pass was carried out by adopting the following cutting parameters suggested for difficult-to-cut alloys: depth of cut 0.25 mm, cutting speed 62 m/min, and feed 0.07 mm/rev. Both flood and cryogenic cooling conditions were used, the latter chosen based on the previous study [6] where cryogenic machining carried out on wrought NiTi was proved to represent a suitable strategy to increase the alloy machinability compared to dry and minimum quantity lubrication cutting conditions. Details about the adopted cryogenic apparatus can be found in a previous work of the Authors [9].

Then, the samples were cut, mounted, polished, and etched in an HF (1 mL), HNO_3 (2 mL), and water (47 mL) solution for 70 s. The microstructure was analysed at different magnifications making use of a EOL™ JSM 7900F HR field emission gun scanning electron microscope (FEG-SEM). To assess the precipitates' nature, energy dispersive spectroscopy (EDS) elemental analyses were performed by means of an Oxford Instrument™ ULTIM MAX 40 probe on unetched polished samples.

Differential scanning calorimeter (DSC) analyses were carried out using a DSC Q200™ machine to determine the NiTi characteristic transformation temperatures *TTs*.

Mechanical characterization was conducted through indentation experiments using an Ultrananoindenter UNHT by Anton Paar™ equipped with a pyramidal Berkovich tip within a distance of 25 µm from the sample surface. A maximum load of 1 mN was applied at a rate of 2 mN/min and kept constant for 10 s to stabilize the time-dependant deformation, then released at the same rate. The elastic modulus and Martens hardness were evaluated following ISO 14,577–1:2015. At least 20 indentations were carried out for each process condition to compute the average values.

In addition, the machined surface topography was assessed by using a Sensofar™ S-Neox optical profiler with a 20X Nikon™ confocal objective. The arithmetic mean height S_a (ISO 25,178–2:2012) on the S-L surface was considered as the baseline parameter for process monitoring, using 2.5 μm S-filter and 0.25 mm L-filter following ISO 16,610–61:2015. Additional areal surface texture parameters, such as Sku, Ssk, Sk, Spk, and Svk, were investigated; however, no significant correlation with the surface properties was found.

3. NiTi characteristics after AM, heat treatment and finish machining

Fig. 2 on the left presents the optical images of the NiTi samples after AM and heat treatment. The AB microstructure consists of equiaxed B2 cubic austenite grains with an average size equal to the hatch spacing (approx. 60 µm). The microstructure of the T3 and T6 heat treated samples is still austenitic, with larger grain size and presence of uniformly distributed precipitates, the latter recognizable in the magnified FEG-SEM images of Fig. 2 on the right. According to the data from the elemental analyses given in at (%), Ni_2Ti_4O Ti-rich precipitates are predominant after the T3 heat treatment, whereas Ni_4Ti_3 Ni-rich precipitates are preferentially formed after the T6 heat treatment. Besides the chemical composition, also the precipitates' size and morphology are strictly dependant on the ageing temperature. Denser and spherical precipitates developed at an ageing temperature of 300 °C since the precipitates' nucleation rate is higher at lower temperatures, but their diffusion rate is lower. At higher temperatures, the opposite effect occurred. When the ageing temperature is 600 °C, the change in the precipitates' morphology from sphere to needle shape corresponds to a decrease in their coherency with the matrix, reducing the strain field associated with the difference between the lattice parameters of the precipitates and matrix.

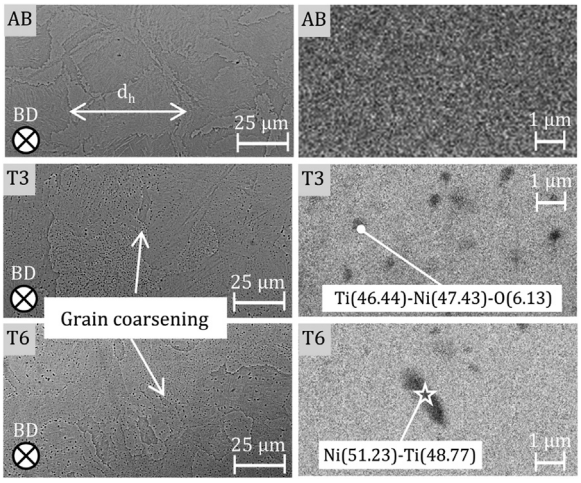

Fig. 2. FEG-SEM micrographs of the AB, T3, and T6 samples are on the left and corresponding magnified images are on the right.

Two examples of DSC curves before and after flood-cooled machining are given in Fig. 3(a), whereas the A_f temperatures extracted from all the DSC curves are reported in Fig. 3(b) at varying process conditions. The DSC curves give the opportunity to calculate

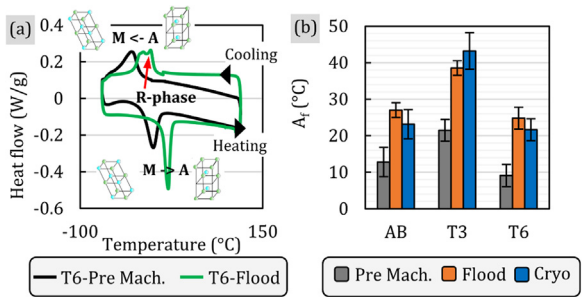

Fig. 3. DSC curves of the T6 samples before and after flood-cooled machining (a); A_f temperatures at varying process conditions (b).

the NiTi TTs. However, since the purpose of the present study is to evaluate the NiTi SE, only the A_f temperature is considered, which must be below room temperature to assure SE.

After both AM and heat treatment, a full austenitic state was achieved at room temperature, being always $A_f < T_{room}$. Compared to the AB case, the T3 heat treatment shifted A_f towards higher values, whereas the T6 condition produced the opposite effect. The increase of A_f at the lowest ageing temperature can be attributed to the precipitates that were formed (see Fig. 2): the higher the density of these precipitates the more the Ni depletion from the matrix, which implies higher TTs [10]. Nevertheless, beyond a threshold temperature value, the Ni atoms diffuse back into the matrix inducing a decrease in A_f, as happened when ageing at 600 °C [10]. It is worth noting that, in any condition before machining, the presence of R-phase peaks in the DSC curves, which are associated with a martensitic transformation that is recognized to unfavourably affect the NiTi SE, was not detected.

Fig. 4(a) shows the loading/unloading characteristics of the three imposed conditions before machining. The precipitates are not only responsible for the TTs shift, but they also influence both the alloy strength and SE. As expected from the DSC results of Fig. 3, the nanoindentation curves differ substantially one from the other. The work recovery ratio η, calculated as the ratio between the recoverable deformation energy and the total one, is presented in Fig. 4(b): compared to the AB condition, it increases by 21% after the T6 heat treatment and decreases by 25% after the T3 heat treatment. This suggests that both the precipitates' composition and coherence with the matrix play a role in affecting the NiTi SE, as the Ti-rich precipitates contribute to inhibiting the crystallographic transformation of austenite into martensite of Fig. 1(a) responsible for the NiTi SE.

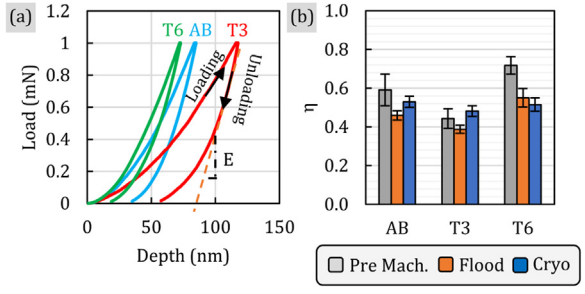

Fig. 4. Force vs. indentation depth curves before machining (a); work recovery ratio η at varying process conditions (b).

Table 2 reports the Martens hardness H at varying process conditions. Before machining, the T6 and T3 heat treated samples exhibit the highest and the lowest hardness, respectively, with one of the AB samples settling in between. Specifically, H was reduced by 48% after the T3 heat treatment and increased by 37% after the T6 heat treatment. The hardness change with respect to the AB condition can be attributed to the formation of precipitates, grain coarsening, as well as the recovery of the AM-induced residual stresses.

The lower hardness shown by the T3 sample compared to the T6 one is due to the formation of Ti-rich precipitates, which are softer with respect to the Ni-rich ones. Nevertheless, the effect of grain coarsening after the T3 heat treatment prevails on the precipitates' hardening when compared with the AB condition.

Fig. 5 shows the cross-section microstructures of the AB, T3 and T6 samples machined under cryogenic cooling conditions. A severe plastically deformed (SPD) layer is clearly visible from the machined surface to the subsurface, regardless of the imposed condition before machining; nevertheless, the T6 sample shows a deeper SPD than the other two conditions. Flood-cooled machined samples present similar, but thinner SPD layers due to the higher cutting temperature reached during machining that favoured the deformation recovery.

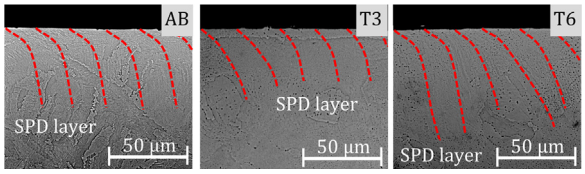

Fig. 5. Microstructure of the AB, T3 and T6 samples after cryogenic machining.

Data reported in Fig. 3(b) and Fig. 4(b) show that, regardless of the heat treatment, finish machining shifted A_f towards higher values and led to the work recovery ratio reduction, which, overall, implies that machining reduces the NiTi SE. This is attributed to the martensite formation during machining, which decreases the amount of austenite that can undergo the transformation of Fig. 1(a). Proof of the martensite formation during machining is the presence of the R-phase peaks on the DSC curves of the machined samples, regardless of the heat treatment (see the DSC curve of the T6 sample after flood machining in Fig. 3(a)).

Contrary to what was expected, the hardness of the AB and T6 samples decreased after machining (see Table 2). This is ascribed to the fact that the lower the A_f temperature the more stable the austenite phase, hence the higher the critical stress required to induce the austenite-to-martensite phase transformation of Fig. 1(a), and, therefore, the material hardness [11]. Therefore, hardness reduction is expected since machining increases the A_f temperatures of the AB and T6 samples. On the contrary, the strain hardening induced by machining in the T3 sample prevails over to the decrease of the critical stress induced by the austenite instability, since, before machining, its A_f temperature is already close to room one. Nevertheless, it is worth noting that, even if reduced, the positive effect of the T6 heat treatment on both the hardness and work recovery ratio is still evident after machining compared to the T3 one. Furthermore, in the case of the T6 sample, cryogenic machining induced a slightly harder surface compared to flood-cooled machining due to the deeper SPD layer induced by the cutting process.

The roughness of the machined surfaces at varying process conditions is reported in Table 3. Compared to flood-cooled machining, the surface roughness of the AB, T3 and T6 cryogenically machined samples was reduced by 7%, 29%, and 15%, respectively, showing a significant effect of the machining cooling conditions, whereas the effect of the heat treatment seems not relevant. Overall, it can be stated that cryogenic machining carried out on T6 heat-treated NiTi allows the

Table 2
Martens hardness H in GPa (standard deviation in brackets) at varying process conditions.

	AB	T3	T6
Pre Mach.	6.58 (1.38)	3.43 (0.47)	8.99 (1.24)
Flood	5.36 (0.33)	3.99 (0.60)	5.23 (0.65)
Cryo	5.02 (0.39)	3.71 (0.51)	5.65 (0.71)

Table 3
Surface roughness S_a in µm (standard deviation in brackets) after machining at varying process conditions.

	AB	T3	T6
Flood	0.31 (0.02)	0.35 (0.01)	0.34 (0.02)
Cryo	0.29 (0.01)	0.25 (0.01)	0.29 (0.01)

enhancement of its surface integrity in terms of both hardness and finish.

4. Potential application

Reaction wheels, which consist of a flywheel, a ball bearing and an electric motor, are widely used in aerospace applications to control the spacecraft's motion without the use of thrusters [12]. Either the ball or the race of the gearing of such wheels, usually subjected to severe wear conditions, can represent an application that would take advantage of NiTi manufactured through the process chain of Fig. 1. NiTi represents indeed an attractive alternative to conventional bearing steels, thanks to its unique characteristics, namely the SE behaviour as well as the high Modell ratio *MR*, which is the ratio between the material hardness and elastic modulus [13]. In particular, the higher the SE and MR the higher the wear resistance thanks to the lower pressure arising from a broader contact area induced by the higher elastic deformation. Such characteristics can provide NiTi the ability to withstand the extreme loads that develop at the contact points between the balls and the inner race of a bearing, without incurring any permanent damage, namely denting (see the scheme of a bearing in Fig. 6(a) where the contact points are indicated when using NiTi or conventional bearing steel).

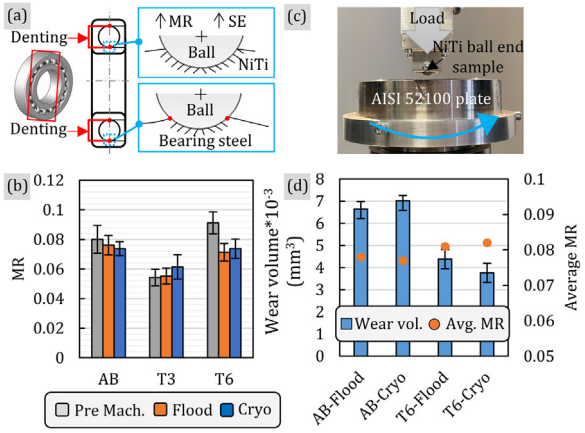

Fig. 6. Scheme of a bearing with the indication of the contact points where denting likely occurs (a); Modell ratio *MR* at varying process conditions (b); wear testing setup (c); wear volume and average *MR* at varying process conditions (d).

For the different process conditions investigated in this study, the *MR* values are plotted in Fig. 6(b) showing that the T6 heat treatment induces a considerably higher MR than the T3 one, both before and after machining. Accordingly, the T3 samples, which also offer the lowest superelastic response, were not tested for the potential application.

The NiTi tribological characteristics were assessed through dry sliding wear tests conducted on a RTEC™ tribometer by adopting a ball-on-plate configuration (see Fig. 6(c)). Ball end samples of 4.6 mm diameter were machined from the AM and T6 heat-treated cylinders adopting the parameters indicated in § 2. The counterpart consists of AISI 52,100 plates, which were polished to achieve a surface roughness S_a of 27.5 ± 3.9 nm. The tribological pair, testing configuration and parameters were chosen to replicate the operating conditions of an actual bearing as closely as possible, having linearized the contact between the ball and the race. The ball end sample was made to rotate counter-clockwise against the plate at a constant speed of 0.03 m/s. A load of 10 N was applied over a time period of 60 min. After the wear tests, the NiTi surfaces were inspected by using the optical profiler to assess the wear volume.

Fig. 6(d) displays the wear volume data at varying process conditions. A remarkable difference is found amongst the AB and T6 conditions, the latter being characterized by 40% lower wear volume on average. On the contrary, the effect played by the finish machining cooling conditions on the wear volume can be considered secondary, even if it is worth noting that, in the case of the T6 condition, the enhancement of the surface integrity induced by cryogenic machining slightly favours the reduction of the wear volume. This secondary effect can be explained by the fact that, during wear testing, after the erosion of the initial surface layers, the influence of the bulk material becomes predominant over that of the surface. Before machining, the T6 samples show, indeed, higher MR and SE with respect to the AB samples. To acknowledge that, besides the wear volume data, Fig. 6 (d) reports the average MR values for the AB and T6 conditions, calculated on the basis of the MR values before and after machining. The correlation shown with the wear volume is remarkable, namely the higher the average MR the lower the wear volume, demonstrating the average MR as a suitable indicator of the NiTi wear behaviour.

5. Conclusions

A process chain including AM, heat treatment and finish machining was adopted to fabricate NiTi samples, showing the significant effect of the process chain parameters on the NiTi surface integrity and superelastic behaviour. In particular, it was evident that the heat treatment after AM induces the formation of precipitates whose type, morphology and size influence the material superelastic response, whereas machining reduces the superelastic characteristics. Nevertheless, cryogenic machining is found to improve the NiTi surface integrity. Results from wear testing in a ball-on-plate configuration show that ageing NiTi at 600 °C after AM coupled with cryogenic finish machining assures the lowest wear volume, thus offering enhanced wear resistance.

Declaration of Competing Interest

The authors declare that they have no known competing financial interests or personal relationships that could have appeared to influence the work reported in this paper.

References

[1] Jani JM, Leary M, Subic A, Gibson MA (2014) A Review of Shape Memory Alloys Research, Applications and Opportunities. *Materials and Design* 56:1078–1113.
[2] Elahinia M, Moghaddam NS, Andani MT, Ameritananzi A, Bimber BA, Hamilton RF (2016) Fabrication of NiTi Through Additive Manufacturing: A Review. *Progress in Materials Science* 83:630–663.
[3] Ma J, Franco B, Tapia G, Karayagiz K, Johnson L, Liu J, Arroyave R, Karaman I, Elwany A (2017) Spatial Control of Functional Response in 4D-Printed Active Metallic Structures. *Scientific Reports* 7:46707.
[4] Xue L, Atli KC, Zheng C, Hite N, Srivstava A, Leff AC, Wilson AA, Sharer DJ, Elwany A, Arroyave R, Karaman I (2022) Laser Powder Bed Fusion of Defect-Free NiTi Shape Memory Alloy Parts with Superior Tensile Superelasticity. *Acta Mater* 229:117781.
[5] Axinte D, Guo Y, Liao Z, Shih AJ, M'Saoubi R, Sugita N (2019) Machining of Biocompatible Materials–Recent Advances. *CIRP Annals–Manufacturing Technology* 68(2):629–652.
[6] Kaynak Y, Tobe H, Noebe RD, Karaca HE, Jawahir IS (2014) The Effects of Machining on the Microstructure and Transformation Behavior of NiTi Alloy. *Scripta Materialia* 74:60–63.
[7] Kaynak Y, Manchiraju S, Jawahir IS, Biermann D (2020) Chip Formation and Phase Transformation in Orthogonal Machining of NiTi Shape Memory Alloy: Microstructure-Based Modelling and Experimental Validation. *CIRP Annals–Manufacturing Technology* 69(1):85–88.
[8] Khademzadeh S, Zanini F, Rocco J, Brunelli K, Bariani PF, Carmignato S (2020) Quality Enhancement of Microstructure and Surface Topography of NiTi Parts Produced by Laser Powder Bed Fusion. *CIRP Journal of Manufacturing Science and Technology* 31:575–582.
[9] Bruschi S, Bertolini R, Ghiotti A, Savio E, Guo W, Shivpuri R (2018) Machining-Induced Surface Transformations Of Magnesium Alloys To Enhance Corrosion Resistance In Human-Like Environment. *CIRP Annals–Manufacturing Technology* 67(1):579–582.
[10] Pelton AR, Dicello J, Miyazaki S (2000) Optimisation of Processing And Properties Of Medical Grade Nitinol Wire. *Minimally Invasive Therapy & Allied Technologies* 9 (2):107–118.
[11] Khanlari K, Shi Q, Hu Li, Hu K, Cao K, Liu P (2021) Effects of Printing Volumetric Energy Densities and Post-Processing Treatments on the Microstructural Properties, Phase Transformation Temperatures and Hardness Of Near-Equiatomic NiTinol Parts Fabricated by a Laser Powder Bed Fusion Technique. *Intermetallics* 131:107088.
[12] Della Corte C (2014) Novel Super-Elastic Materials for Advanced Bearing Applications. *Adv. Sci. Technol. Trans Tech. Publ. Ltd*, 1–9.
[13] Oberle TL (1951) Properties Influencing Wear of Metals. *Journal of Metals* 3:438.